9.11 A SIMPLE CONCEPTUAL MODEL OF LOWER TROPOSPHERE STABILITY AND MARINE STRATUS AND STRATOCUMULUS CLOUD FRACTION

Yanping He and Robert Dickinson

Georgia Institute of Technology, Atlanta, Georgia

1 INTRODUCTION

Marine Stratus and Stratocumulus (MSC) play fundamental roles in the global radiation budget, ocean-atmospheric coupling, and the mean atmospheric circulation. Its cloud albedo can significantly affect the amount of radiation reaching the earth surface; its strong cloud top radiative cooling is the main driver for the cloud-top boundary layer turbulence over the cold ocean surface; the persistence of MSC over the subtropical ocean surface enhances the latitude gradient of atmospheric long wave radiative cooling and reinforce the radiation forcing for the tropical atmospheric circulation (Rossby and Zhang 1995; Tian & Ramanathan 2001).

The development of realistic cloud cover parameterization in a global climate model is a major challenge, and current GCMs and reanalysis systems have serious problems in simulating MSC (Keihl 1998, Jakob 1999, Siebesman et al 2003).

Most present cloud cover schemes in GCMs have been relative humidity (RH) based, as proposed initially by Smagorinsky (1960). RH is a good indictor of cloud cover when most of the air in a GCM grid box is saturated or near saturated. MSC is a thin cloud with thickness from100m to 500m. For a GCM grid box of approxmately1000m thick, most of air in the box should be dry air. For such a dry grid box, RH structure can no longer be a good indicator for the cloud cover. The thermal structure becomes at least as important as the moisture structure. Physically consistent prognostic cloud schemes have been developed for GCMs to directly link the cloud thermophysics to cloud radiative properties and the boundary layer turbulence (Tiedtke 1993, Tompskins 2001).

*Corresponding Author Address: Yanping He, Scholl of Earth and Atmospheric Science, Georgia Institute of Technology, Atlanta, GA 30332; e-mail: yhe@eas.gatech.edu

In these prognostic cloud schemes, RH is still the dominate prediction factor. These schemes are not only computational expensive, but also depend on variables such as rates of entrainment and detrainment, and cloud water advection, which are difficult to be verified and interpreted. Another trend in current large scale cloud simulation is to complicate the parameterization by introducing the sub-grid variability using a statistical cloud cover scheme (Tompkins, 2001). The advantage of this method is that the RH-based cloud cover scheme is no longer “all-or-nothing”; the disadvantage of this method is that the statistical scheme is highly depend on both the choice of its probability distribution function (PDF) and the grid-averaged RH. Cloud Resolving Model (CRM) results are widely used to decide PDFs. However, even in CRM, MSC is parameterized. As a result of, the choice of PDF is lack of physical insight. Another disadvantage of using statistical cloud cover scheme for MSC is that it is computationally expensive. A better cloud cover scheme should be able to minimize the infinite dimensions into as few dimensions as possible, but capture and represent the key feedbacks between cloud and large scale environment.

As early as 1980, Slingo found an empirical relationship between cloud fraction and atmosphere stability (defined as the potential temperature difference between 700mb and ocean surface) based on GATE observations (1960). Klein’s study in 1993 also found an empirical linear relationship between the seasonal variation of MSC cloud cover and the seasonal variation of atmospheric stability globally except for the Arctic. Such a linear relationship between cloud cover and atmospheric stability has been used in the NCAR CAM cloud cover scheme and many simple models to simulate cloud and to study atmospheric-cloud interaction in climate sensitivity and global warming (NCAR CAM document; Clement & Seager, 1999; Larson, Hartmann, and Klein, 1999). The colder the SST, the greater the atmospheric stability, the larger the boundary layer cloud cover, and the weaker the solar flux reaching the ocean surface. It suggests a negative

feedback between cloud cover and SST. However, in the southeast Pacific, the MSC is rapidly developed during the transition season of May and June, and maintains its maximum value from June to October; while atmospheric stability gradually reaches its maximum in September and October, three months later.

From Fig.28 in Keihl et al 1998, the observed seasonal variation of MSC cloud cover has a "two steady states and one jump" pattern. The NCAR CCM empirical cloud cover scheme predicts the MSC peak is at the coldest SST seasonal in September, but the observed seasonal maximum of MSC begins from the transition season of May and June. Why does the linear relationship between MSC cloud cover and atmospheric stability fail to explain the annual cycle of MSC in the southeast Pacific? What physical processes link the atmospheric stability to the subtropical MSC? What are the fundamental rules determining the development and dissipation of MSC in the subtropics on monthly and seasonal timescales?

Subtropical MSC are formed in the descending branch of tropical large scale circulation over the cold ocean surface. Their development and the dissipation are closely linked to the strong large scale subsidence, cloud top-entrainment instability, surface flux, and drizzle (Lilly, 1968; Randall, 1980, 1984; Betts, 1990; Bretherton, 1997; Steven, 2000). Observational relationships between marine cloud cover and large scale state variables have been studied in time scales of synoptic, monthly, seasonal, interannual and decades (Bajuk, Louis, and Leovy, 1998a, 1998b; Klein, Hartmann, and Norris, 1994; Klein, 1997; Norris, 1994; Norris, 1997; Norris and Leovy, 1994), but no single predictor could explain more than 20% of the observed cloud cover variance, particularly in the shorter time scales.

In the cold SST season (June to November), the atmospheric stability is large, the large scale subsidence is strong, maximum solar radiation is located in the northern tropics, a large amount of dry energy is transported into the boundary layer. MSC is at its seasonal maximum, with strong cloud radiative cooling at the boundary layer top. In the warm SST season (January to May), atmospheric stability is small, large scale subsidence is weak, a small amount of dry energy is transported from above into the boundary layer; MSC is at its seasonal minimum, and its cloud top radiative cooling is small. During the transition season of May to June, MSC are quickly developed from seasonal minimum to seasonal maximum; the surface latent heat flux greatly increases. Nigam (1997) suggested a positive feedback among cloud top radiation cooling, southerly surface wind tendency, and the latent heat flux in explaining the development of MSC near the Peruvian region. A positive correlation between MSC cloud cover and surface latent heat flux is also suggested in the observational study of Klein, Hartmann and Norris (1994). According to the above physical picture, large cloud top radiative cooling is positively linked to the large amount of dry energy input from the free atmosphere and the surface latent heat flux. Therefore, we hypothesize that the role of boundary layer cloud is to keep the boundary layer dry energy in balance. Based on this idea and observations, a physical-based cloud cover scheme is formulated.

The structure of this paper is as following: In section 2, the dataset used is briefly described; in section 3, we take results from regional analysis of the seasonal variation of cloud distribution, clear sky and cloudy radiative forcing within atmosphere, and surface latent heat flux to suggest that the role of boundary layer cloud is to keep the lower troposphere into dynamical-radiative-convective equilibrium; then in section 4, we formula the low cloud fraction based on lower atmospheric stability and large scale subsidence driven by the annual cycle of clear sky radiative cooling; in section 5, offline experiments using ISCCP FD dataset and ERA-40 reanalysis suggest that the new cloud fraction scheme could better simulate the low cloud cover variation in monthly and seasonal time scales; in section 6, NCAR CAM3.1 simulation results using new cloud cover scheme is discussed; and conclusions follow in section 7.

2 DATASET

2.1 ISCCP FD dataset

The 3-hour daily ISCCP FD dataset used in this study was developed by Rossow W.B. and Y.C. Zhang on a 2.5 lat x 2.5 long global grid and at five pressure levels (surface, 680mb, 440mb, 100mb, TOA) during January 1985-December 2000. This dataset contains not only the satellite measured radiative flux at the top of atmosphere and at the surface, but also contains the vertical profiles of radiative flux obtained using satellite measured cloud information and radiative transfer model. It contains 3-hour cloud cover information, and sea surface temperature from 1985 to 2000. ISCCP FD dataset is obtained directly from Y.C. Zhang and W.B. Rossow. The information on the data inputs and data quality can be found in Rossow W.B. and Y.C. Zhang (1995) and Zhang Y.C. and W.B. Rossow (1995).

2.2 ERA-40 reanalysis

The daily values of surface flux, air temperature, specific humidity, and relative humidity at 1000 mb, and air temperature at 700mb used in this study are obtained from ERA-40 website at http://data.ecmwf.int/data/d/era40_daily/. The study period is from January 1985 to December 2000. The publications related to ERA-40 data quality can be found from the following website at http://www.ecmwf.int/publications/library/do/references/list/192.

2.3 NCEP-NCAR reanalysis

The monthly mean data of surface fluxes, temperature, specific humidity and RH at 1000 mb, and 700mb are obtained from NCEP-NCAR reanalysis during January 1985 to December 2000. The dataset is obtained from climate diagnostics center. The dataset is discussed in details in (Kalnay et al, 1996).

2.4 MSC study regions

This study focuses on the following four subtropical regions:

MSC regions	Location
Peruvian	$5^\circ - 20^\circ S, 80^\circ - 95^\circ W$
Namibian	$5^\circ - 20^\circ S, 5^\circ W - 10^\circ E$
California	$17.5^\circ - 32.5^\circ N, 120^\circ - 135^\circ W$
Canirian	$12.5^\circ - 27.5^\circ N, 22.5^\circ - 37.5^\circ W$

Table 1. The geographical extent of four subtropical MSC regions in this study.

3 The MODEL DESCRIPTIONS

The lower troposphere below trade wind inversion at around 700 mb is assumed to be in convective-radiative-dynamical equilibrium for the monthly and seasonal time scales. The dry static energy equation and moist equation may be written as

$$R_{crf} = A(\theta) + Q_c + F_{SH} - R_{clr} \qquad (1)$$

$$Q_c - L\,P = 0 \qquad (2)$$

$$L\,P = \beta\,F_{LH} \qquad (3)$$

where $A(\theta)$ is the vertically integrated dynamical transport of dry static energy from surface to 700 mb, Q_c is the total convective heating within the lower troposphere, R_{full}, R_{clr}, R_{crf} are respectively the full sky radiative cooling , the clear sky radiative cooling, and the cloud radiative cooling, P is precipitation, β is local precipitation coefficient, we set $\beta = 0.3$, F_{LH} and F_{SH} are surface latent heat flux. The dynamical transport of dry static energy and convective heating is balanced by clear sky radiative cooling and cloud radiative cooling. Moist equation is the balance between net evaporation and precipitation.

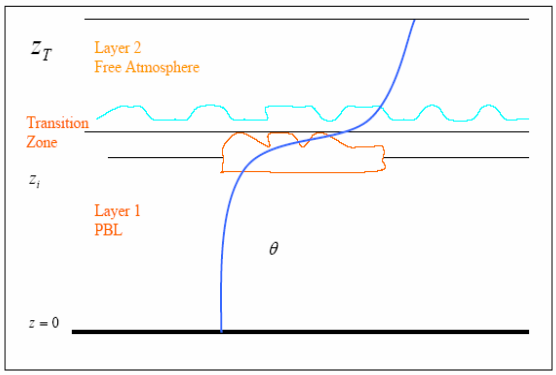

Fig.1 A conceptual two-layer structure for lower troposphere in subtropical MSC regions.

The lower troposphere in the subtropical MSC regions can be simplified as a two layer structure which is shown in Fig. 1. A cold, moist boundary layer topped by a dry warm free air below 700 mb. Boundary layer cloud is formed at the top of the boundary layer capped with a strong temperature inversion. The large subsidence is assumed to be unchanged from boundary layer height to 700mb, the potential temperature is assumed to be little changed within the boundary layer. The dynamical transport of dry static energy becomes

$$A(\theta) = -c_p\ \overline{w}_{925}\left(\theta_{700} - \theta_{srf}\right) + A_H(\theta) \qquad (4)$$

$$A_H(\theta) = -\vec{V}_{925} \bullet \nabla\theta\ \Delta z_1 - \vec{V}_{775} \bullet \nabla\theta\ \Delta z_2 \qquad (5)$$

where θ_{700} and θ_{srf} are respectively potential temperature at 700 mb and ocean surface, Δz_1 is

layer thickness from surface to 850 mb, Δz_2 is the layer thickness from 850mb to 700mb.

We calculated the annual mean dry static energy balance using ERA-40 and ISCCP-FD data during 1985 to 2000 for each term in equation (1), the results are shown in Table 2, the unit is W/m^2.

	$A_z(\theta)$	$A_H(\theta)$	βF_{lh}	F_{sh}	R_{clr}	R_{crf}
Peruvian	48	-19.8	37.0	14.0	-77.4	-16.6
Namibian	33.6	3.7	35.9	13.9	-74.9	-19.7
California	45.6	-18.1	36.6	16.9	-67.4	-13.4
Canirian	21.7	-14.0	44.9	11.5	-65.5	-5.6

Table2 Calculated Annual Mean Dry Static Energy Budget in Lower Troposphere during 1985-2000.

From table 2, the dominated heating source in lower troposphere is the vertical transport of dry static energy and convective heating; the dominated heating sink is the clear sky radiative cooling. Assuming sensible heat and horizontal advection are secondary in the dry static energy balance, equation (1) combined with equation (4) becomes

$$R_{crf} = -c_p \ \overline{w}_{925}\left(\theta_{700} - \theta_{srf}\right) + Q_c - R_{clr} \quad (6)$$

where $\nabla\theta = \theta_{700} - \theta_{srf}$ is defined as the atmosphere stability in this study.

4 A SIMPLE CLOUD COVER SCHEME BASED ON ATMOSPHERIC STABILITY

Cloud radiative forcing within the lower atmosphere is defined as in equation (7) and calculated from ISCCP FD 3-hour radiative profile data in four subtropical regions at 2.5 X 2.5 spatial resolutions

$$R_{crf} = R_{full}^{b680} - R_{clear}^{b680} \quad (7)$$

where R_{full}^{b680} and R_{clear}^{b680} are respectively the full sky and clear sky radiative cooling from surface to 680 mb. From Fig. 2, there are solid linear relationships between daily ISCCP low cloud cover and daily cloud radiative forcing within lower troposphere in four subtropical MSC regions. The cloud radiative forcing can be described as the function of low cloud cover.

$$R_{crf} = A_c R_{crf}^0 - R_0 \quad (8)$$

As shown in Fig. 2, the unit area cloud radiative forcing $R_{crf}^0 = 70 \quad w/m^2$, $R_0 = 20\, w/m^2$. The seasonal variation of cloud radiative forcing within atmosphere represents the seasonal variation of low cloud cover in subtropical regions.

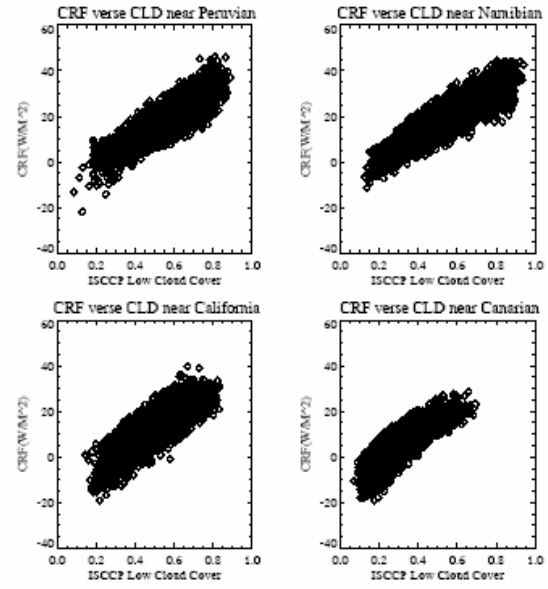

Fig. 2 ISCCP-FD monthly cloud radiative forcing within lower troposphere verse the ISCCP monthly low cloud cover in four subtropical MSC regions during 1985-2000.

A simple cloud cover formula can be derived from equations (1) an (6)

$$A_c = (-c_p \ (\overline{w}_{925}\left(\theta_{700} - \theta_{srf}\right) + \beta F_{LH} - R_{clr} + R_0) / R_{crf}^0 \quad (7)$$

Where R_{crf}^0 is the unit area cloud radiaitve forcing within lower troposphere. Because the surface latent heat flux is determined by ocean surface temperature, near surface relative humidity, and surface wind speed. The surface wind speed could further be controlled by atmosphere stability. Therefore the surface latent heat flux is highly dependent on lower troposphere stability. The large scale subsidence is controlled by slowly varying

annual cycle of solar heating, the fast propagation of wave, and noise. In order to capture the seasonal variation of cloud, the 6 hour ERA-40 large scale subsidence is smoothed by 30 day averaged when simulating the cloud cover.

4.1 Surface evaporation parameterization

We use the bulk parameterization for the surface latent heat flux:

$$\overline{w'q'}^{0} = C_E \overline{U}_a (q_s - q_a) = C_E \overline{U}_a q_s (1 - RH) \quad (8)$$

The surface latent heat flux is determined by the turbulence coefficient C_E, surface wind speed V, and the near surface humidity difference $q_s - q_a$.

Monthly surface wind speed at 2m is plotted in Fig. 3 as a function of monthly atmospheric stability in 0.25° C bin width using daily ERA-40 reanalysis data (solid line) and monthly NCEP-NCAR reanalysis data (dot-dashed line) in four Subtropical MSC regions during 1985 to 2000. A nearly linear relationship between the surface wind speed and the atmospheric stability is suggested through both ERA-40 and NCEP-NCAR reanalysis in four subtropical MSC regions. There is approximately 0.15 m/s surface wind speed increase for every 1 degree increase of atmospheric stability.

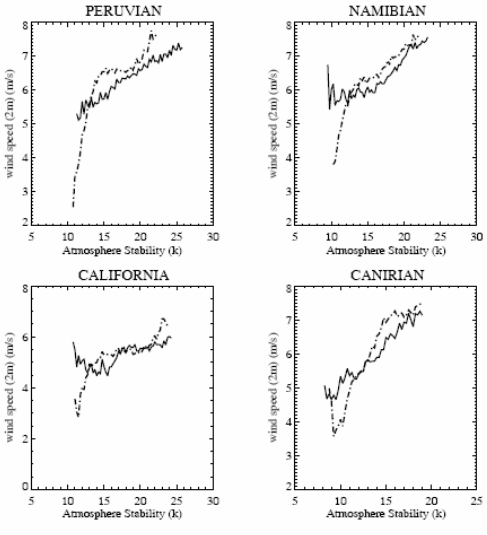

Fig. 3 Monthly surface wind speed at 2m as a function of monthly atmospheric stability in 0.25° C bin width using daily ERA-40 reanalysis data (solid line) and monthly NCEP-NCAR reanalysis data (dot-dashed line) in four Subtropical MSC regions during 1985 to 2000.

The surface humidity difference is determined by ocean surface temperature and near surface relative humidify which is defined by $RH = q_a / q_s$. In this study, the near surface relative humidity is calculated using ERA-40 daily dew point temperature at 2m and ocean surface daily SST using ISCCP-FD data. Monthly near surface RH is plotted in Fig. 4 as a function of monthly atmospheric stability in 0.25° C bin width using daily ERA-40 reanalysis data (solid line) and monthly NCEP-NCAR reanalysis data (dot-dashed line) in four Subtropical MSC regions during 1985 to 2000. ERA-40 RH is calculated using ERA-40 2m dew point temperature at 2m and SST from ISCCP FD data. The NCEP-NCAR RH is calculated using NCEP specific humidity at 2m and NCEP skin temperature. It is shown from the figure that surface relative humidity has strong positive relationship with atmospheric stability. The near surface relative humidity increases 2.5% when atmosphere stability increases 1K. The reason is that stronger stability isolates the warm and dry free air mixing into the boundary layer, and it also enhances the moisture transport from surface, so the near surface relative humidity is high. The combined saturated humidity effect and the surface relative humidity effect leads to a negative trend of near surface humidity difference with atmospheric stability in the subtropical ocean, which is supported with ERA-40, NCEP-NCAR, and ISCCP-FD data analysis shown in Fig. 5.

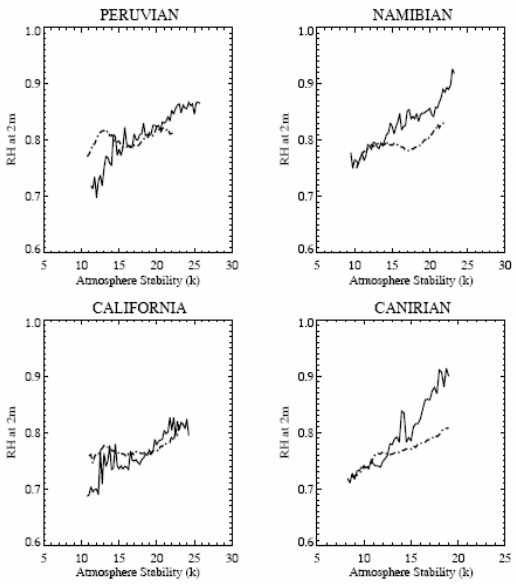

Fig. 4 Monthly surface relative humidity (rh = qa / qs) at 2m as a function of monthly atmospheric stability in 0.25° C bin width using daily ERA-40 reanalysis data (solid line) and monthly NCEP-NCAR reanalysis data (dot-dashed line) in four Subtropical MSC regions during 1985 to 2000.

This negative trend can be simplified as the following linear relationship:

$$q_s - q_a = \Delta q_0 \left(1 - \frac{\Delta\theta}{\Delta\theta_{\max}} \right) \qquad (9)$$

Where $\Delta\theta_{\max}$ is the stability capacity, its physical meaning is that when the atmospheric stability is larger than the maximum stability capacity, the atmosphere is no longer gain the moisture from the ocean surface.

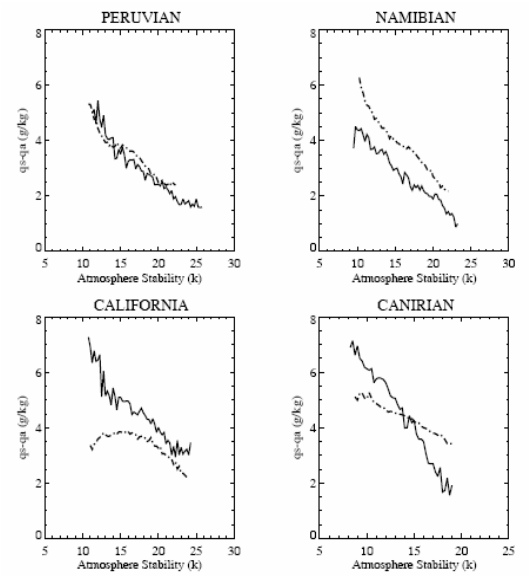

Fig. 5 Monthly specific humidity difference at 2m as a function of monthly atmospheric stability in 0.25° C bin width using daily ERA-40 reanalysis data (solid line) and monthly NCEP-NCAR reanalysis data (dot-dashed line) in four Subtropical MSC regions during 1985 to 2000.

According to the above analysis, we simplify the surface latent heat flux as

$$L_v \rho_a \overline{w'q'}^0 = b\Delta\theta \left(1 - \frac{\Delta\theta}{\Delta\theta_{\max}} \right) + c \qquad (10)$$

where b and c are statistical coefficients determined by ocean surface properties. Fig. 6 is the relationship between surface latent heat flux and lower troposphere stability using 1985-1989 ERA-40 daily data in four subtropical MSC regions. In low stability region, the stability effect in surface wind speed determines that the surface latent heat increases with the increasing stability. However, after the stability reaches a critical value, the stability effect on near surface relative humidity becomes more important. Increasing atmosphere stability will decrease the surface latent heat flux.

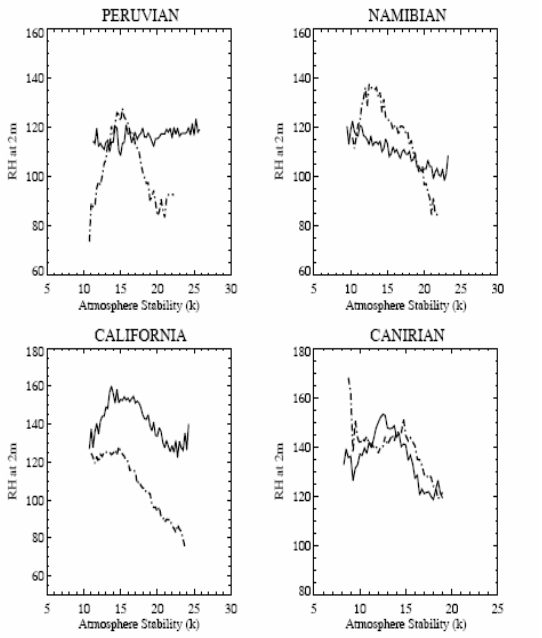

Fig. 6 Monthly surface latent heat flux (W/m^2) as a function of monthly atmospheric stability in 0.25° C bin width using daily ERA-40 reanalysis data (solid line) and monthly NCEP-NCAR reanalysis data (dot-dashed line) in four Subtropical MSC regions during 1985 to 2000.

4.3 The derived cloud cover formula

Combing equations (7) and (10) we get

$$A_c = a(-\overline{w}_a)\Delta\theta + b\Delta\theta \left(1 - \frac{\Delta\theta}{\Delta\theta_{\max}} \right) - Q_0 \qquad (11)$$

where a, b are empirical coefficients, Q_0 is determined by clear sky radiative cooling and ocean surface properties.

Fig. 7 clearly demonstrates the difference between two cloud cover schemes. Nonlinear cloud cover scheme diagnoses the largest cloud cover when

the atmospheric stability reach a critical value, here is 20K, then the cloud cover decreases with the increasing atmospheric stability. However, linear cloud cover scheme diagnoses the largest cloud cover when the atmospheric stability is largest. Therefore, comparing with the nonlinear cloud cover scheme, the linear cloud cover scheme tends to underestimate cloud cover in small and moderate stability regime and overestimate the cloud cover in large stability regime.

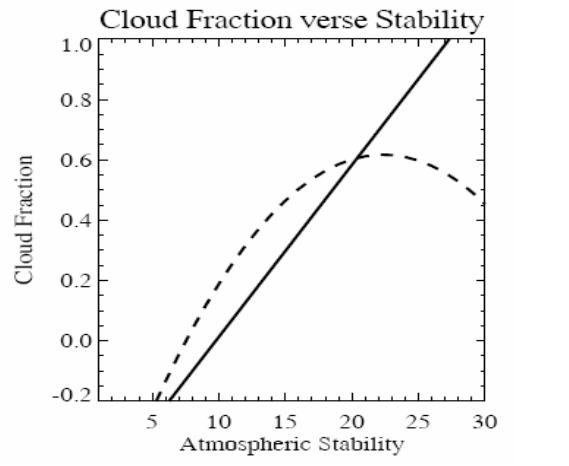

Fig. 7 Cloud cover as a function of atmospheric stability. The solid line is calculated using NCAR CAM3.1 empirical linear relationship between low stratiform cloud cover and atmosphere stability; the dashed line is the cloud cover calculated using eq. (20) assuming constant large scale subsiding rate.

5 OFFLINE SIMULATIONS OF LOW STRATIFORM CLOUD COVER NEAR THE WESTERN COAST OF CONTINENTS

In both dependent simulation and independent validation experiments, the empirical constants are derived from 1985-1989 dependent simulation. We use ISCCP-FD daily SST data field and ERA-40 daily temperature field at 700 mb to compute the daily atmosphere stability. Then we simulate the daily and monthly cloud cover over four subtropical MSC regions using both NCAR empirical cloud cover scheme, and the new cloud cover scheme.

5.1 Experiment 1: atmospheric stability

5.1.1 Dependent simulations (1985-1989)

In this experiment, the simulated cloud cover depends only on atmospheric stability. The large scale subsidence is given its area-averaged annual mean value obtained from ERA-40 vertical velocity at 925 mb, Q_0 is given a constant value based on annual mean clear sky radiative cooling R_{clr} and R_0 . The empirical coefficients in equation (11) are derived using ISCCP daily low cloud cover from 1985 to 1989 and least-square technology in Table 3.

	$\Delta\theta_{max}$	a $\overline{w}$ (1e-3)	b	Q_0
Peruvian	30.5	3	5.6	55
Namibian	33	2.7	6	55
California	34	2.0	5.8	45
Canirian	23.5	2.0	6.3	45

Table 3 Empirical coefficients used in experiment 1.

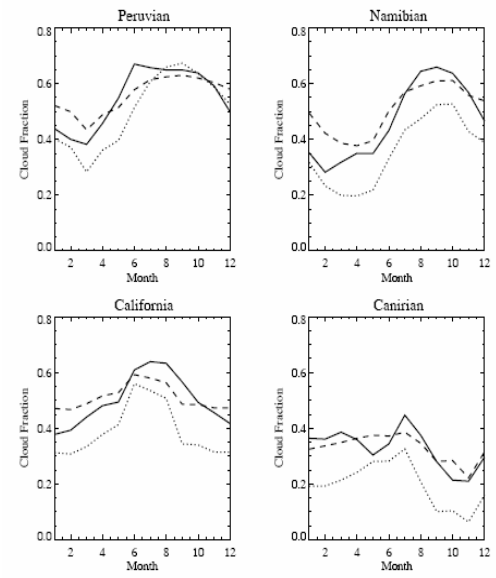

Fig. 8 Regional averaged seasonal cycle of monthly mean low cloud cover in the southeast Pacific during 1985 to 1989. The solid line is ISCCP monthly low cloud cover, thick dashed line is simulated cloud cover using new scheme, the thin dashed line is the cloud cover simulated using the linear relationship.

Fig. 8 is the regional averaged seasonal cycle of monthly mean low cloud cover in the southeast Pacific during 1985 to 1989. Comparing with NCAR cloud cover scheme, the new scheme simulates better the seasonal amplitude and the

seasonal phase near the Peruvian region and Namibian regions. ISCCP monthly cloud reaches its maximum at June and July, the new scheme reaches its maximum in July and August, but the NCAR scheme reaches its maximum in September and October. From Fig. b, c, d, there are moderate improves in the simulation of season variation of cloud cover near California, Namibian, and the Canarian.

5.1.2 Independent validations (1990-2000)

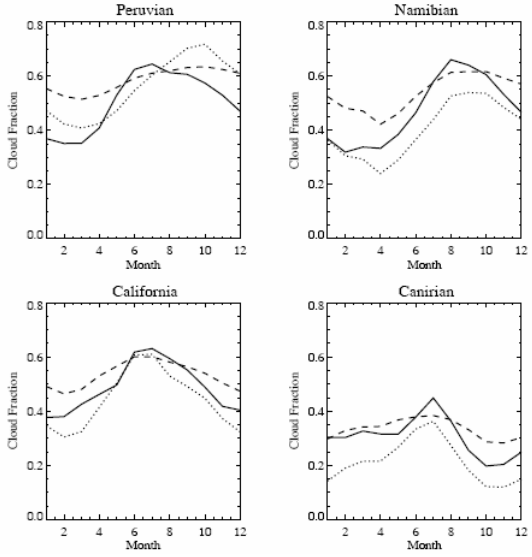

Fig. 9 is the comparison of seasonal cycle of area- averaged monthly mean cloud cover simulated by NCAR MSC cloud cover scheme (thin dashed line), the new scheme (thick dashed line), and the ISCCP monthly low cloud cover (solid line).

Fig. 9 is 11-year averaged seasonal variation of area-averaged monthly cloud cover in four MSC regions from 1990 to 2000. Comparing with monthly ISCCP low cloud cover, NCAR cloud cover scheme much underestimates MSC cloud cover from May to July by 10% and much overestimate MSC cloud cover from September to December by 10% near the Peruvian region. The new scheme simulates well in the cold SST seasons, but overestimates cloud cover in the warm SST season.

5.2 Experiment 2: large scale subsidence near Peruvian region

In this experiment, cloud cover is simulated based on the atmospheric stability and large scale subsidence near the Peruvian region.

$$A_c = a(-\overline{w}_{925})\Delta\theta_{700} + b\Delta\theta\left(1-\frac{\Delta\theta_{700}}{\Delta\theta_{\max}}\right) - Q_0 \quad (12)$$

ERA-40 6 hour vertical velocity at 925 mb is smoothed through 30-day averaged. We use the similar empirical coefficient as in exp. 1, $a = 1.15$, $b = 5.6$ Q_0 =55.

5.2.1 Dependent simulation

When ERA-40 large scale subsidence is used as input, the new scheme significantly improves the seasonal cycle in both seasonal amplitude and the seasonal phase near the Peruvian region.

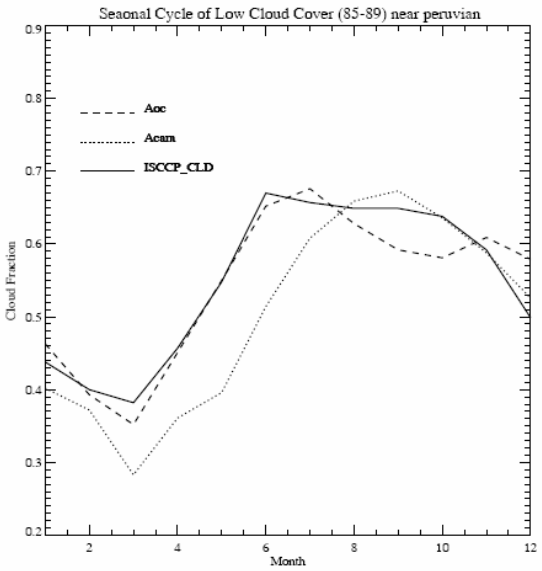

Fig. 10 The seasonal cycle of area-averaged low cloud cover near Peruvian region averaged during 1985 to 1989 by ISCCP (solid line), new scheme (thick dashed), and NCAM linear scheme (thin dashed).

5.2.2 Independent validation

Fig. 11 is 11-year averaged seasonal variation of area-averaged monthly cloud cover in four MSC regions from 1990 to 2000. Comparing with results from experiment 1, the simulated seasonal variation of cloud cover becomes much realistic, with realistic seasonal amplitude and seasonal phase.

In Fig. 12, upper panel is the simulated area-averaged monthly low cloud cover from 1990 to 2000 by ISCCP (SOLID), new scheme (thick dashed), NCAM linear scheme (thin dashed); the middle panel

is the simulated cloud cover by NCAR linear scheme verse ISCCP cloud cover; the lower panel is the simulated low cloud cover using new cloud scheme verse ISCCP cloud cover. The correlation between NCAR simulated 11-year area-averaged monthly cloud cover and ISCCP area-averaged monthly cloud cover is 40%; while the correlation for the new scheme is 60%. The ISCCP monthly cloud cover is gradually decreased in the late 1990s. The NCAR linear scheme could not capture this trend; while the new scheme simulates well this negative trend because of both large scale subsidence effect and nonlinear atmospheric stability effect.

The implementation of ERA-40 large scale subsidence on cloud cover scheme could not improve the simulation of low cloud cover in other three regions. The preliminary results of data analysis energy balance in those regions suggest that the horizontal transport of dry static energy become more important and its seasonal variation is not in phase with the seasonal variation of vertical transport of dry static energy.

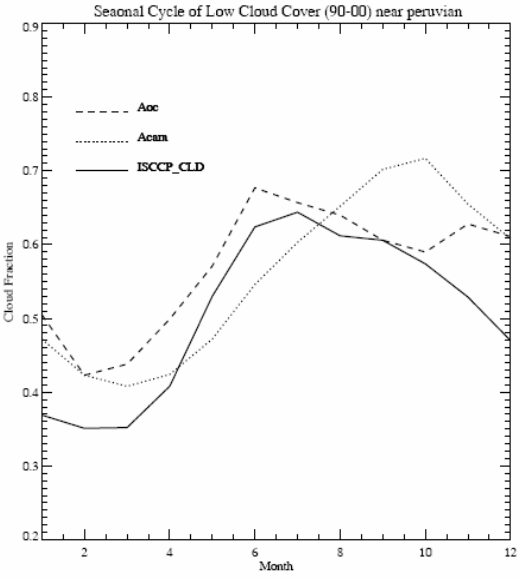

Fig. 11 The seasonal cycle of area-averaged low cloud cover near Peruvian region averaged during 1990 to 2000 by ISCCP (solid line), new scheme (thick dashed), and NCAM linear scheme (thin dashed).

7 SUMMARY

The parameterization of the seasonal variation of marine stratus and stratocumulus in large scale models can be represented using only lower troposphere stability. Previous linear empirical relationship between cloud cover and stability is widely used in GCMs and simple box models. However, they lack the physical insight and fail to explain the seasonal phase of MSC near the southeast Pacific. In this study, we provide physical pictures to link atmosphere stability and boundary layer cloud cover in all subtropical MSC regions.

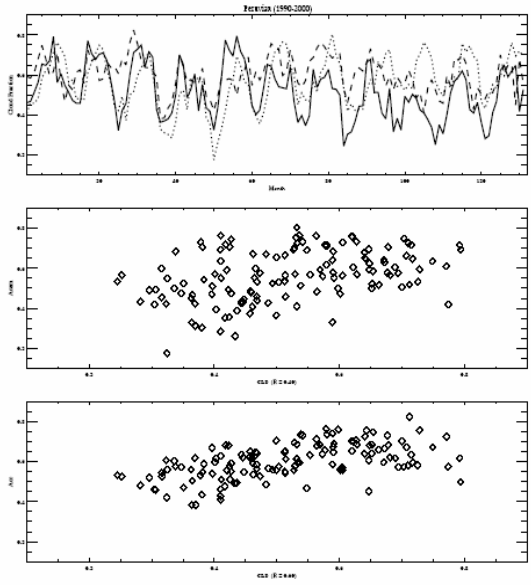

Fig. 12 Upper panel is the simulated area-averaged monthly low cloud cover from 1990 to 2000 by ISCCP (SOLID), new scheme (thick dashed), NCAM linear scheme (thin dashed); the middle panel is the simulated cloud cover by NCAR linear scheme verse ISCCP cloud cover; lower panel is the simulated low cloud cover using new cloud scheme verse ISCCP cloud cover.

In our conceptual model, MSC is formed in the subtropical large scale subsidence regions. When the large amount of dry static energy is transported from above into the boundary layer and latent heat released from ocean surface, cloud is developed to radiate back the extra energy into space to keep the lower troposphere in radiative-convective-dynamical equilibrium. The seasonal variation of vertical transport of dry static energy and surface latent heat release lead to the seasonal variation of cloud top radiative cooling, which is a linear function of low cloud cover. This physical picture is supported by ISCCP FD data, ERA-40 reanalysis, and NCEP-NCAR reanalysis. A diagnostic low cloud cover scheme is developed based on the above physical pictures, which is a nonlinear function of atmospheric stability and large scale subsidence. Offline

experiments show that the new scheme perform much better than the empirical linear low stratiform cloud cover scheme, which is widely used from simple box models to general circulation models. This new scheme can be easily implemented into large scale models and simple conceptual models.

8 ACKNOWLEDGEMENTS

This study is funded by NSF No. ATM 0343485.

9 REFERENCES

Bajuk, Louis and C. B. Leovy, 1998a: Are there real interdecadal variations in marine low clouds, *J. Climate*, **11**, 2910-2921.

--------- and C. B. Leovy , 1998b: Seasonal and interannual variations in stratiform and convective clouds over the tropical pacific and Indian oceans from ship observations, *J. Climate*, **11**, 2922-2941.

Betts A.K., 1990: A cloudiness transition in a marine boundary layer, *J. Atmos. Sci*., **47**, 1480 -1497.

Bretherton C. and M.C. Wyant, 1997: Moisture transport, lower-troposphere stability, and decoupling of cloud-topped boundary layer, *J. Atmos. Sci*., **54**, 148-167.

Clement A. and R. Seager, 1999: Climate and the tropical oceans, *J.Climate*, **13**, 3383-3401.

Deardorff J.W., 1980: Cloud top entrainment instability, *J. Atmos. Sci*., **37**, 131-147.

Dima I. and J.M. Wallace, 2003: On the seasonality of the Hadley cell, *J. Atmos. Sci.* **60**, 1522-1526.

Jakob C., 1999: Cloud cover in the Europe Reanalysis, *J.Climate*. **12**, 947-959.

E. Kalnay, M. Kanamitsu, R. Kistler, W. Collins, D. Deaven, L. Gandin, M. Iredell, S. Saha, G. White, J. Woollen, Y. Zhu, A. Leetmaa, B. Reynolds, M. Chelliah, W. Ebisuzaki, W. Higgins, J. Janowiak, K.C. Mo, C. Ropelewski, J. Wang, Roy Jenne and Dennis Joseph, 1996: The NCEP-NCAR 40-year reanalysis project, *BAMS*, **77**, 437-471.

Klein S.A. and D. L. Hartmann, 1993: The seasonal cycle of low stratiform clouds, *J. Climate*, **6**, 1587-1606.

----------, D. L. Hartmann, and J. R. Norris, 1994: On the relationships among low-cloud structure, sea surface temperature, and atmospheric circulation in the summertime northeast pacific, *J.Climate* , **8**, 140-1155.

--------, 1997: Synoptic variability of low-cloud properties and meteorological parameters in the subtropical trade wind boundary layer, *J.Climate*, **10**, 2018-2039.

Kiehl J.T., J.J. Hack, and J. W. Hurrell, 1998: The energy budget of the NCAR Community Climate Model: CCM3, *J. Climate*, **11**, 1151-1178.

Larson K. and D. L. Hartmann, 1999: The role of clouds, water vapor, circulation, and boundary layer structure in the sensitivity of the tropical climate, *J. Climate*,**13**, 2359-2374.

Lilly D.K, 1968: Models of cloud-topped mixed layers under a strong inversion, *Q.J.R.Meteor. Soc*., **94**, 292-309.

Nigam S., 1997: The annual warm to cold phase transition in the eastern equatorial pacific: diagnosis of the role of stratus cloud-top cooling, *J. Climate*, **10**, 2447-2467.

Norris J.R., 1994: On the relationships among low-cloud structure, sea surface temperature, and atmospheric circulation in the summertime northeast pacific, *J. Climate*, **8**, 1140-1155.

---------- and C. B. Leovy, 1994:Interannual variability in stratiform cloudiness and sea surface temperature, *J. Climate*, **7**, 915-1925.

----------, 1997: Synoptic variability of low-cloud properties and meteorological parameters in the subtropical trade wind boundary layer, *J. Climate*, **10**, 1018-1039.

Randall D.A., 1980, Entrainment to stratocumulus layer with distributed radiative cooling, *J. Atmos. Sci.*, **37**, 148-159.

Stevens B., W. R. Cotton, G. Feingold, and C. Moeng, 1998, Large-eddy simulations of strongly precipitating, shallow, stratocumulus-topped boundary layers, *J. Atmos. Sci.*, **55,** 3136-3638.

Rossow W.B. and Y.C. Zhang, 1995:Calculation of surface and top of atmosphere radiative fluxes from physical quantities based on ISCCP data sets 2 validation and first results, *JGR*, **100**, D1, 1167-1197.

Siebesma A. Pier, et al, 2003: Cloud representation in general circulation models over the northern pacific ocean: A EUROCS intercomparison study, *Q.J.R.Meteorol. Soc*., submitted 2003.

Slingo J.M., 1987:The development and verification of a cloud prediction scheme for the ECMWF model, *Q.J.R.Meteorol. Soc*., **113**, 899-927.

Smagorinsky, J., 1960: On the dynamical prediction of large-scale condensation by numerical methods. *Geophys. Mon.*, **5**, 71-78.

American Geophysical Union, Washington, U.S.A.

Smith R.N.B., 1990: A scheme for predicting layer clouds and their water content in a general circulation model, *Q.J.R.Meteorol. Soc.*, **116**, 435-460.

Teixeira J., 2001, Cloud Fraction and relative humidity in a prognostic cloud fraction scheme, *Monthly Weather Review*, **129**, 1750-1753.

Tian B. and V. Ramanathan, 2001:Role of tropical clouds in surface and atmospheric energy budget, *J. Climate*, **15**, 296-305.

Tiedtke M., 1993: Representation of clouds in large-scale models, *Monthly Weather Review*, **12**, 3040-3061.

Trenberth K.E. and D.P. Stepaniak,, 2003, Seamless poleward atmospheric energy transports and implications for the Hadley circulation, submitted to *J.Climate*, **16**, 3705-3721.

Tompkins A., 2001: A prognostic parameterization for the subgrid-scale variability of water vapor and clouds in large-scale models and its use to diagnose cloud cover, *J. Atmos. Sci.*,***59***, 1917-1942.

Zhang Y.-C., W. Rossow and A.A. Lacis, 1995: alculation of surface and top of atmosphere radiative fluxes from physical quantities based on ISCCP data sets 1 method and sensitivity to input data uncertainties, *JGR*, **100**, D1. 1149 -1165.

Zhang M.H., W. Y. Lin,1 S. A. Klein, J. T. Bacmeister, S. Bony, R. T. Cederwall, A. D. Del Genio, J. J. Hack, N. G. Loeb, U. Lohmann, P. Minnis, I. Musat, R. Pincus, P. Stier, M. J. Suarez, M. J. Webb, J. B. Wu,1 S. C. Xie, M.-S. Yao, and J. H. Zhang, 2005: Comparing clouds and their seasonal variations in 10 atmospheric general circulation models with satellite measurements, *JGR*, **10**, D15S02, 1-18.